CRYSTAL GROWTH & DESIGN

Article

pubs.acs.org/crystal

Probing Structural Changes in a Phosphonate-based Metal–Organic Framework Exhibiting Reversible Dehydration

Tiffany L. Kinnibrugh,*[,†] Ayi A. Ayi,[‡] Vladimir I. Bakhmutov,[†] Jerzy Zoń,[§] and Abraham Clearfield*[,†]

[†]Department of Chemistry, Texas A&M University, College Station, Texas 77842-3255, United States

[‡]Department of Pure and Applied Chemistry, University of Calabar, P.M.B 1115-Calabar, Nigeria

[§]Faculty of Chemistry, Wroclaw University of Technology, 50-370 Wroclaw, Poland

Supporting Information

ABSTRACT: A one-step hydrothermal synthesis with small amines and 1,3,5-benzenetriphosphonic acid was used to prepare single crystals of isostructural anionic metal–organic frameworks (MOF): $Zn_{2.5}(H)_{0.4-0.5}(C_6H_3O_9P_3)(H_2O)_{1.9-2}(NH_4)_{0.5-0.6}$ and $Zn_{2.5}(H)_{0.75}(C_6H_3O_9P_3)(H_2O)_2(CH_3NH_3)_{0.25}$. The ammonium ions are exchangeable with lithium ions. The MOF exhibits reversible dehydration, and the process was studied by two complementary methods: solid state NMR and in situ X-ray diffraction. These experiments revealed three different phases. The crystal structures of all phases have been determined, showing loss in volume of the structure due to a phase change. The ammonium ions remain in the structure and are forced to occupy the larger pores due to a reduction in free volume. The change in positions of the guest molecules in the framework has an effect on the potential conductivity properties of the materials. Changes in framework and guest molecules due to negative expansion have an effect on other physical and chemical properties and need to be explored.

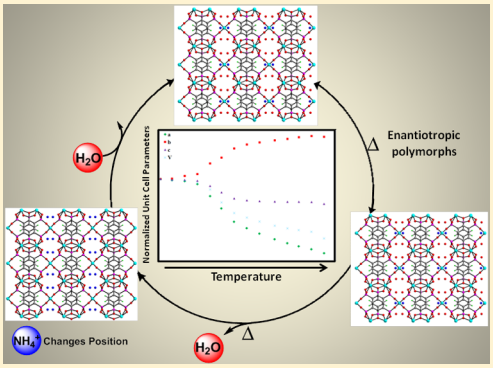

INTRODUCTION

The immense research in metal–organic frameworks (MOFs) is due to the wide potential in applications owing to the diversity in topological architectures.[1−7] The differences in chemical and physical properties of their pores make MOFs selective for particular guest molecules. External stimuli can alter the structure of a material and thereby the physical properties.[8−13] This has an influence on the selectivity of guest molecules and the arrangement of guest molecules in MOFs. Both temperature and pressure are external stimuli that have an impact on the structures.[8,11−15] In particular, negative thermal expansion (NTE) is an isochemical process where, upon heating, the volume of the material decreases and has been observed in silicates, zirconium tungstate, zeolites, and other materials.[16−19] MOFs have also been reported to exhibit negative thermal expansion.[20−22] The IRMOFs have been described as one of the most contracting materials known,[20] and many studies are still being carried out investigating this phenomenon for MOF-5 and HKUST-1.[21−27] Studies showing negative expansion in porous materials have focused on the change in structure versus temperature.[20,21,25] However, little is known about how the guest molecules respond under these same conditions.

In MOFs that exhibit negative thermal expansion, the overall structure shrinks upon heating, resulting in smaller pores.[20,25] For functional materials with proton or ion carriers occupying the pores, the loss in free volume could alter the positions of the guest molecules, thereby changing the conductive properties. The positions of the guest molecules in high temperature structures are important, due to the challenge of developing MOFs with high conductivity at elevated temperatures (up to 120 °C) required for fuel-cell hydrogen-conversion technology.[28]

Monitoring the changes in the guest molecules and framework can be carried out using in situ X-ray diffraction and solid-state nuclear magnetic resonance (NMR). This allows mapping of the guest molecule positions throughout the negative thermal expansion process. The relative stability of the guest molecules in proton-conducting MOFs over a range of temperatures allows for these types of studies to be carried out.[28−31]

Nontraditional inorganic–organic metal phosphonates synthesized using the ligand 1,3,5-benzenetriphosphonic acid (BTP) have been investigated for their proton conducting properties.[32] A layered material, PCMOF-3, with an extended microstructure of water molecules was formed using Zn(II) ions and BTP.[32] The material provided modest conductivity data due to constrained intergrain proton transfer.[32] An anionic form was also prepared using large cation ions.[33] A layered material (LBP-II) was also found for lanthanum ion and BTP.[34] However, the use of BTP with Cu(II) ions formed a three-dimensional (3D) framework where water molecules protrude

Received: March 18, 2013
Revised: May 2, 2013
Published: May 3, 2013

into the pores, leading to a promising proton-conducting material.[35] To extend PCMOF-3 to a 3D structure, a topotactic pillaring approach of anionic layers was used.[36,37] This resulted in four semicrystalline versions of the extended-PCMOF-3.

Reported herein, are the crystal structures of two anionic 3D frameworks with small amines as countercations, $Zn_{2.5}(H)_{0.4-0.5}(C_6H_3O_9P_3)(H_2O)_{1.9-2}(NH_4)_{0.5-0.6}$ (ZnBP−NH_4) and $Zn_{2.5}(H)_{0.75}(C_6H_3O_9P_3)(H_2O)_2(CH_3NH_3)_{0.25}$ (ZnBP−CH_3NH_3), resulting from the hydrothermal synthesis using Zn(II) cations and BTP. This approach differs from the topotactic pillaring approach; however, a similar structure was obtained.[36] Several types of protons are present within the pores (ammonium ions, acid protons, and water molecules). The reversible dehydration process was investigated with solid state NMR and in situ X-ray diffraction. The experiments showed that the material shrinks upon heating, reducing the free volume of the pores and thus altering the positions of the solvent molecules. The negative expansion is a result of a phase change due to the loss in water molecules.

EXPERIMENTAL SECTION

Commercially available reactants were used without further purification. The ligand 1,3,5-benzenetriphosphonic acid was synthesized according to a previous procedure.[35]

Synthesis of ZnBP-NH_4. The material $Zn_{2.5}(H)_{0.4-0.5}(C_6H_3O_9P_3)(H_2O)_{1.9-2}(NH_4)_{0.5-0.6}$ was hydrothermally synthesized (autogenous pressure for 6 days) at 160 °C from a mixture of zinc oxide (Aldrich, 98%), HCl (Fisher Scientific), ligand BTP, potassium acetate (Fisher Scientific), urea (EM Science), and H_2O/dioxane. In a typical synthesis of I, ZnO (0.100 g, 1.2 mmol) was dispersed in 2 mL of water, followed by the addition of 0.52 mL HCl and 1.68 mL 1,4-dioxane. To this mixture was added BTP (0.100 g, 0.31 mmol), urea (0.120 g, 2.0 mmol), and potassium acetate (0.180 g, 1.8 mmol). The resulting suspension with a pH of 1 was sealed in a Teflon-lined steel autoclave and heated at 160 °C for 6 days. The product, a crop of colorless platelike crystals was filtered and washed with distilled water and dried at ambient temperature. Yield: 0.143 g (87.1% based on BTP). Elemental analysis (%) and ICP-AES: calcd (%), C, 13.79; N, 1.58; H, 1.88; P/Zn ratio, 1.20 and exptl (%), C, 13.97; N, 1.57; H, 1.51; P/Zn ratio, 1.25.

Synthesis of ZnBP−CH_3NH_3. The compound $Zn_{2.5}(H)_{0.75}(C_6H_3O_9P_3)(H_2O)_2(CH_3NH_3)_{0.25}$ was synthesized by a similar procedure as that of compound ZnBP−NH_4, except that urea was replaced with 1,3-dimethylurea. In a typical synthesis, ZnO (0.100 g, 1.2 mmol) was dispersed in 2 mL of water followed by the addition of 0.52 mL HCl and 1.68 mL 1,4-dioxane. To this mixture was added BTP (0.100 g, 0.31 mmol), 1,3-dimethylurea (0.174 g, 2.0 mmol), and potassium acetate (0.180 g, 1.8 mmol). The resulting suspension with a pH of 1 was sealed in a Teflon-lined steel autoclave and heated at 160 °C for 7 days. The product, a crop of colorless platelike crystals was filtered and washed with distilled water and dried at ambient temperature. Yield: 0.109 g (66.5% based on BTP). Elemental analysis (%) and ICP-AES: calcd (%), C, 14.4; N, 0.67; H, 1.79; P/Zn ratio, 1.20 and exptl (%), C, 14.1; N, 0.62; H, 1.21; P/Zn ratio, 1.23.

Ion Exchange, ZnBP−Li. The material $Zn_{2.5}(C_6H_3O_9P_3)(H_2O)_2(Li)_{1.31}(OH)_{0.31}$ was obtained by dispersing ZnBP−NH_4 (0.239 g, 0.46 mmol) and $LiOH{\cdot}H_2O$ (0.049 g, 1.17 mmol) in 65 mL DI water and refluxing for 40 h. The solution was then filtered and washed with 250 mL of DI water. Yield: 0.169 g. Elemental analysis (%) and ICP-AES: calcd (%), C, 13.8; N, 0.0; H, 1.36; P/Zn ratio, 1.20; P/Li ratio, 3.00 and exptl (%), C, 13.6; N, 0.0; H, 1.23; P/Zn ratio, 1.20; P/Li ratio, 2.29.

Materials Characterization. Thermogravimetric analyses were carried out on a T.A. Instrument TGA Q-500. The samples were heated from 25−1000 °C, using a heating rate of 5 °C/min with a 90/10 air/N_2 flow. Elemental analysis for carbon, nitrogen, and hydrogen (C, N, and H) was performed by Atlantic Microlab, Inc. Compositional analysis for zinc, phosphorus, and lithium was carried out, using a Anderson Analytical ICP-AES. To prepare a typical sample, 0.033 g was dissolved in 40 μL of conc. HCl, 40 μL of conc. HNO_3, and 20 mL of DI water, which was then shaken overnight. A Mettler Toledo polymer DSC equipped with a liquid nitrogen cooling system and 50 mL/min purge of dry nitrogen gas. Samples (~3 mg) were weighed into 40 μL aluminum pans and subjected to one heating cycle at 5 °C/min over the various ranges.

Solid-State NMR Dehydration−Hydration Study. The $^{31}P\{^1H\}$, CP $^{31}P\{^1H\}$, CP $^{13}C\{^1H\}$, and ^1H MAS NMR experiments were performed with a Bruker Avance-400 spectrometer (400 MHz for ^1H), using a standard 4 mm MAS probe head. Standard one pulse (direct nuclear excitation) and/or standard cross-polarization pulse sequences were applied in these experiments at relaxation delays necessary for a quantitative analysis of the spectra. The MAS NMR spectra have been recorded with variations in the spinning rates between 5 and 14 kHz. The external standards used for calculations of chemical shifts of ^{13}C and ^{31}P nuclei were TMS and H_3PO_4 solution, respectively. The ^1H chemical shifts were determined by direct addition of CH_3OH into the sample and recalculated relative to TMS. The ^1H T_1 measurements were performed with a standard inversion−recovery pulse sequence where RF pulses were carefully calibrated. The ^1H relaxation data were treated with a standard program.

To study the dehydration process, a ZnBP−NH_4 sample was heated under vacuum to 300 °C for 24 h on a Quantachrome degasser. The sample was rehydrated by exposing it to the atmosphere overnight. Both ^1H and ^{31}P MAS NMR were recorded at each step of the experiment: initial, dehydration, and rehydration. Elemental analysis for carbon, nitrogen, and hydrogen was acquired for the first step (%): C, 13.97; N, 1.57; H, 1.51 and third step (%): C,13.93; N, 1.41; H, 1.36.

Crystallographic Studies. *Structure Determination from Single Crystals Data.* Single crystal data were collected on a Bruker-AXS Apex II CCD X-ray diffractometer (Mo Kα radiation, λ= 0.71073 Å), operating at 110 K. Crystallographic parameters and experimental details are given in Table S1 of the Supporting Information. The structures were solved by direct methods and refined by the full-matrix least-squares technique against F^2 with the anisotropic displacement parameters for all nonhydrogen atoms. Hydrogen atoms were added in idealized positions and refined using a riding model with $U_{iso} = nU_{eq}$ for carbon atoms connected to the relevant H atom, where n = 1.2 for H atoms. Hydrogen atoms on water molecules and ammonium nitrogen were found using a difference map and refined using a riding model with $U_{iso} = nU_{eq}$, where n = 1.5. Anisotropic displacement parameters were established for all nonhydrogen atoms. The following programs were utilized: cell refinement and data reduction, SAINT;[38] semiempirical method for absorption correction, SADABS;[39] structure solution, SHELXTL;[40] molecular graphics, Diamond[41] and Mercury.[42]

For compound ZnBP−CH_3NH_3, the carbon and nitrogen atoms in the methyl ammonium ion are positionally disordered.

In Situ X-ray Diffraction Hydration Study. All synchrotron powder diffraction data for the in situ X-ray diffraction hydration experiments were recorded on 1-BM-C at Advance Photon Source (APS), Argonne National Laboratory (Argonne, IL) with an average beamline wavelength of 0.6124 Å. Data collection was performed with a Perkin-Elmer flat-panel area detector (XRD 1621 CN3-EHS) over the angular range of 1−25° 2θ.

Samples were loaded in a kapton capillary (0.9 mm diameter), which was attached to the flow-cell setup for in situ synchrotron powder X-ray diffraction (PXRD) measurements.[43] The samples were heated at a heating rate of 3 K min^{-1} with a He gas flow to reach the target temperature and then cooled down to 298 K. To rehydrate the materials at 298 K, the samples were exposed to water vapor with a He gas flow.

Structure Determination of Phase II and Phase III for ZnBP−NH_4. Two phases were identified during the in situ X-ray diffraction experiments, and the structure for each phase was determined from a PXRD pattern at a specific temperature (phase II at 333 K and phase III at 423 K).

A set of approximately 20 Bragg peaks were used by the index procedure[44] in TOPAS.[45] Evaluation of the unit cell and all possible space groups were analyzed by the "profile-matching mode" (Le Bail decomposition[46]) with TOPAS.[45] Analysis for systematic absences and best profile matching led to the correct space groups. The initial models were found by direct space methods in FOX.[47,48] The initial model was found using the following scattering units: two zinc atoms, one rigid BTP unit without free orientation and two water molecules, and an ammonium molecule without hydrogen atoms with free orientation and position in the unit cell. The initial coordinates for all scattering units were taken from the single crystal data of ZnBP−NH_4. For phase III of ZnBP−NH_4, no water molecules were included in the initial model. The parallel tempering algorithm was used by the global optimization procedure.

The synchrotron PXRD data were used in the Le Bail decomposition to refine the unit cell and profile parameters in JANA2006.[49] The background was defined using 20 Chebyshev polynomials. The peak-shape profiles were defined by a pseudo-Voigt function. The structure was refined by the Rietveld method. The crystallographic and refinement parameters are given in Table S2 of the Supporting Information. Hydrogen atoms were geometrically placed and fixed before the final refinement. Rietveld plots are given in Figures S1−S4 of the Supporting Information. The BTP unit was restricted to geometrically correct values. For phase III, the Simpson correction was applied for asymmetry.

RESULTS

Crystal Structure of ZnBP−NH_4. The ZnBP−NH_4 MOF crystallized in the orthorhombic *Ibam* space group. The asymmetric unit consists of two Zn(II) ions, a BTP molecule sited on a center of symmetry with one-half of the molecule as the asymmetric portion, a water molecule, and an ammonium ion. The structure of ZnBP−NH_4 is a 3D framework built from layers linked by ZnO_4 tetrahedra (Figure 1). The structure is

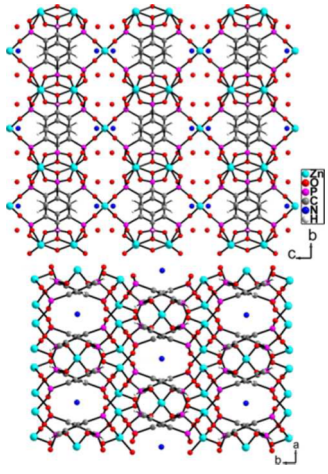

Figure 1. Views of the crystal structure along the *a* axis (top) and *c* axis (bottom) of ZnBP−NH_4.

not a traditional pillared material where the inorganic layer is linked by organic groups. Instead, the ZnO_4 centers act as pillars that link an inorganic−organic layer together. The layer is built from Zn(II) ions in tetrahedral coordination-linking columns of BTP molecules. The columns are formed from roughly parallel π-stacked dimers of BTP molecules along the *a* axis (d···d, distance = 8.472 Å). In the π-stacked dimers, the BTP molecules are rotated 180° to each other with a $\pi\cdots\pi$ distance of 3.672 Å. For each BTP molecule, one phosphonate group (P2) lies parallel to the layer and the others (P1) are rotated 60° into the interlayer. Within the intralayer, the phosphonate oxygen atoms from a BTP molecule coordinate to eight ZnO_4 centers (Zn1−O = 1.905 −2.006 Å). The phosphorus oxygen atom, O2, does not coordinate the intralayer ZnO_4 centers. The ZnO_4 center, situated above the layer, is coordinated only to the oxygen atom, O2, from four symmetry equivalent BTP groups (Zn2−O2 = 1.930(3) Å). The Zn2 sites act as pillars, linking the inorganic−organic layers. The interlayer distance is 9.908 Å, corresponding to half of the *c* axis.

The 3D framework forms two types of pores that interconnect (Figures 1 and 2). The pores are formed from

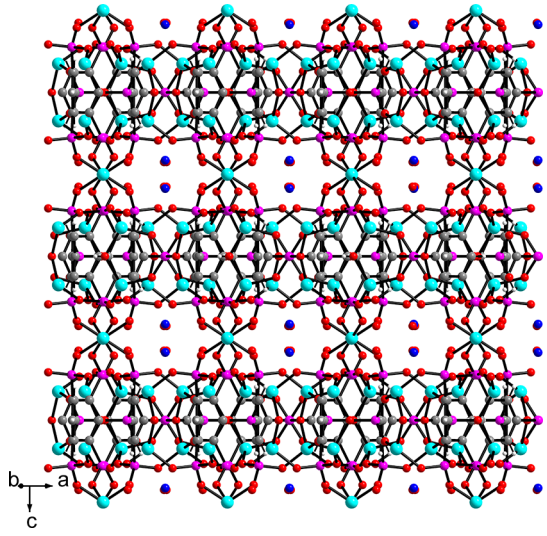

Figure 2. View of the smaller pores running along the [110] direction, which interconnects the larger pores. The organic−inorganic layers and the ZnO_4 pillars can be clearly seen. The solvent molecules are disordered.

the spaces between the ZnO_4 pillars. The larger pore runs along the [100] direction, and the smaller pores run along the [110] direction and interconnect the larger pores. Both pores are filled with water and ammonium ions. The ammonium ions compensate the −1 charge on the ZnBP framework. The formula determined from the single crystal data, $Zn_{2.5}(H)_{0.4-0.5}(C_6H_3O_9P_3)(H_2O)_{1.9-2}(NH_4)_{0.5-0.6}$, is in good agreement with the formula derived from elemental analysis $[Zn_{2.5}(H)_{0.41}(C_6H_3O_9P_3)(H_2O)_2(NH_4)_{0.59}]$. In both cases, the NH_4/ZnBP ratio is less than one, therefore the framework must be partially protonated to have a charge balance.

A topotactic pillaring approach resulted in the same compound; however, single crystals were not obtained.[36] Determination of the structure from powder diffraction data resulted in the space group *Iba*2; however, we find from single crystal data that the space group is *Ibam*. Determination between *Iba*2 and *Ibam* from powder diffraction data is difficult because these groups are indistinguishable by systematic absences. The determination of the position for the ammonium ion and water molecules is difficult. Previously, from powder diffraction data, the ammonium ion positions were reported in the larger pores.[36] Reported herein, are two structures where the ammonium ion occupies a position first in the small pore (ZnBP−NH_4, phase Ia) and then in the larger pore (ZnBP−NH_4, phase Ib). The site occupancy of the ammonium ion is restricted to 0.25 for phase Ia, which results in slightly less %N than determined by elemental analysis. The methyl ammonium

dx.doi.org/10.1021/cg400399v | *Cryst. Growth Des.* 2013, 13, 2973−2981

ion also occupies the same position as ammonium ion in phase Ia and is described below. The refinement parameters for phase Ia are slightly better (Table S1 of the Supporting Information). However, it is believed that the ammonium ions can occupy either positions and therefore the solvent molecules are disordered.

Crystal Structure of ZnBP−CH_3NH_3. The ZnBP−CH_3NH_3 MOF crystallized in the orthorhombic *Ibam* space group (Table S1 of the Supporting Information). The asymmetric unit consists of two Zn(II) ions, a BTP molecule sited on a center of symmetry with one-half of the molecule as the asymmetric portion, a water molecule, and a methyl ammonium ion. The framework is isostructural to the ZnBTP framework (Figure 3). 1,3-Dimethylurea decomposed into

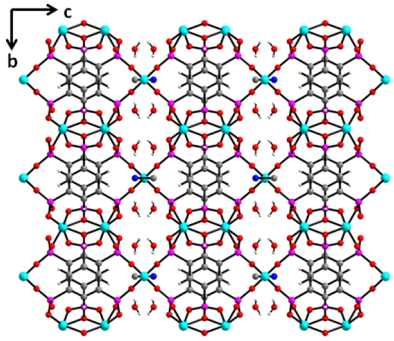

Figure 3. A view of the crystal structure along the *a* axis for ZnBP−CH_3NH_3. The CH_3NH_3 molecules are disordered.

methyl ammonium ions. The carbon and nitrogen atoms in the methyl ammonium ion are positionally disordered and occupy two symmetry-equivalent sites of the NH_4 ion in the ZnBP−NH_4 MOF. The formula was determined to be $Zn_{2.5}(H)_{0.75}(C_6H_3O_9P_3)(H_2O)_2(CH_3NH_3)_{0.25}$, indicating that the framework must be protonated to obtain charge balance.

Ion Exchange: ZnBP−Li. The replacement of NH_4^+ ions in the ZnBP−NH_4 materials was carried out by refluxing the material with $LiOH{\cdot}H_2O$. Refluxing helps drive the reaction by removing NH_3 from the solution. The material remained crystalline under the basic conditions (pH 10, Figure S5 of the Supporting Information). The TGA is similar to that of ZnBP−NH_4, where initially water loss occurs. However, there is no loss due to NH_3, owing to their replacement by Li^+ ions (Figure 4). For ZnBP−NH_4, weight loss due to NH_3 occurs between 320 and 460 °C. Both materials have high thermal stability (~600

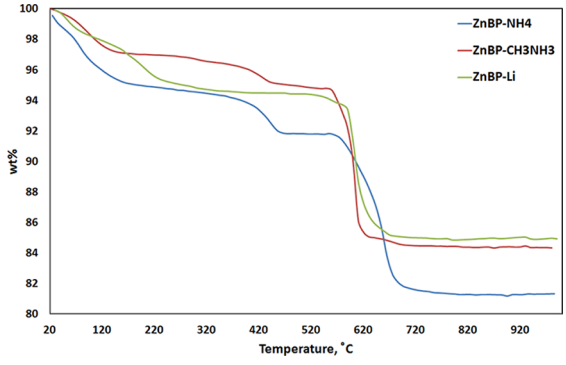

Figure 4. Thermogravimetric analysis of compounds ZnBP−NH_4, ZnBP−CH_3NH, and ZnBP−Li.

°C). The difference wt% loss in the TGA from decomposition is consistent with the different compositions. On the basis of ICP, the resulting material has the following formula $Zn_{2.5}(C_6H_3O_9P_3)(H_2O)_2(Li)_{1.31}(OH)_{0.31}$.

Solid-State NMR Studies. The $^{31}P\{^1H\}$ MAS NMR experiment, performed with a single-pulse proton-decoupled sequence for freshly prepared compound ZnBP−NH_4 spinning at 10 kHz shows two resonances at 19.3 and 13.2 ppm. In excellent agreement with the X-ray structure, their integral intensities are related as 1 to 2 (Figure 5). Both of the signals

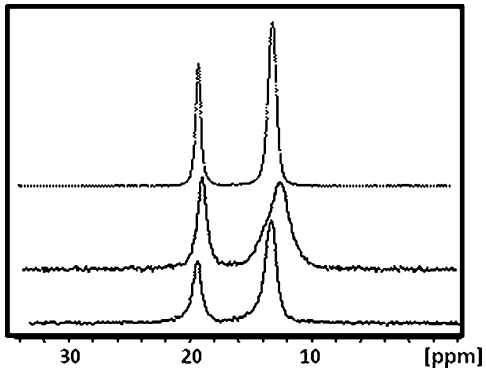

Figure 5. The $^{31}P\{^1H\}$ MAS NMR spectra recorded for ZnBP−NH_4 at a spinning rate of 10 kHz from top to bottom: a fresh-prepared ZnBP-NH_4, the thermally treated (~300 °C) ZnBP−NH_4 just after heating, and the thermally treated ZnBP−NH_4 after 14 h.

are symmetric and relatively sharp with line widths of 70 and 122 Hz, respectively, and accompanied by low intensity sidebands. The slightly larger broadening of the high-field resonance is obviously connected with a larger local disorder around the phosphorus atoms participating in the formation of cavities. The presence of NH_4^+ ions and H_2O molecules in the cavities could explain the slight increase in the relative intensity of the high-field resonance in the cross-polarization ^{31}P MAS NMR experiment.

Finally, nonequivalency of phosphorus atoms in the $^{31}P\{^1H\}$ MAS NMR spectra of ZnBP−NH_4 corresponds to appearance of numerous signals in the well-resolved $^{13}C\{^1H\}$ CP MAS NMR spectrum of ZnBP−NH_4, spinning at a rate of 10 kHz. The spectrum shows at least three $^{13}C-P$ doublet resonances at 130.9, 130.5, and 126.3 ppm with $^1J(C-P)$ constant of 184, 185, and 194 Hz, respectively. It is interesting that in the solid state these constants are larger than in solutions.[35] A group of ^{13}C lines, observed at 132.7−132.6 ppm, obviously illustrates the absence of fast rotation of the aromatic rings, leading to the observation of two signals in solution only.[35]

The $^{31}P\{^1H\}$ MAS NMR spectrum recorded just after thermal treatment of ZnBP−NH_4 (Figure 5) reveals the following spectral changes: the low-field, still-symmetric resonance broadens to 126 Hz, shifting insignificantly to 19.0 ppm, while the high-field resonance becomes broad (262 Hz) and nonsymmetrical, showing shoulders, and undergoes a high-field displacement to 12.4 ppm. Generally, such changes correspond to increasing amorphous character of the sample,[50] where after heating, a local disorder increases for the phosphorus atoms forming cavities. However, after 14 h, the $^{31}P\{^1H\}$ MAS NMR spectrum shows recovered structural regularity, and the two initial phosphorus resonances are again observed at the same chemical shifts (Figure 5).

dx.doi.org/10.1021/cg400399v | *Cryst. Growth Des.* 2013, 13, 2973−2981

The phase transition of ZnBP−NH_4 can be well-traced by ^{1}H MAS NMR (Figure 6). The initial sample shows two broad ^{1}H

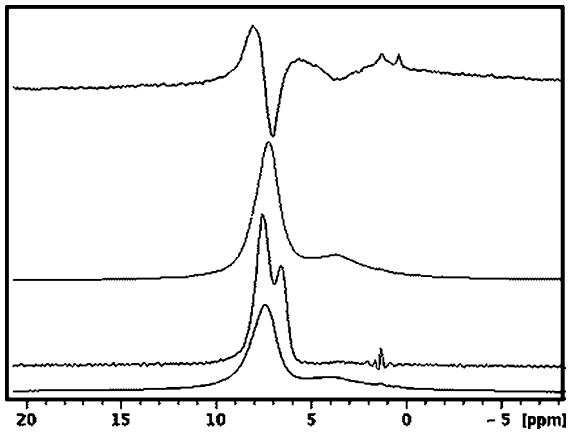

Figure 6. The ^{1}H MAS NMR spectra of ZnBP−NH_4 spinning at 10 kHz from top to bottom: the partially relaxed spectrum obtained for fresh-prepared ZnBP−NH_4 at a delay time of 1 s, the single-pulse spectrum obtained for fresh-prepared ZnBP−NH_4, the single-pulse spectrum obtained for ZnBP−NH_4 in 30 min after heating (the FID is treated with a Gauss function to increase resolution, and the single-pulse spectrum obtained for ZnBP−NH_4 in 14 h after heating.

resonances centered at 7.3 and 3.6 ppm. Their integral intensity ratio is determined as 2.9 to 1. Just after the thermal treatment, the high-field signal (3.6 ppm) completely disappears and the low-field broad line transforms to two resonances centered at 7.6 and 6.6 ppm (Figure 6) with intensities related to 2:1. Then after 14 h, as in the case of ^{31}P MAS NMR, the ^{1}H MAS NMR spectrum again converts to the initial spectrum to show two resonances at 7.4 and 3.8 ppm (Figure 6).

To better understand the nature of these signals and thus to make ^{1}H signal assignments, we have performed inversion−recovery (^{1}H T_1) experiments for ZnBP−NH_4 (before heating and after its structural recovery), spinning at 10 kHz. The experiments carried out for a freshly prepared sample of ZnBP−NH_4 have shown that both of the ^{1}H resonances (7.4 and 3.6 ppm) relax very similarly, and their spin−lattice relaxation is not exponential. The relaxation curves can successfully be treated with a stretched exponential,[50,51] $I = I_0\{1-2\exp[-(\tau/T_1)^{\beta}]\}$ (Figure 7), where the β parameter takes the values of 0.73 (δ = 7.4 ppm) and 0.68 (δ = 3.6 ppm) and T_1 times are calculated as 1.5−1.3 s for both lines. Note that such β parameters could be caused by a partial contribution of spin diffusion into spin−lattice relaxation.[50] It is interesting that after the structural recovery both of the ^{1}H resonances again relax similarly but the nonexponential character of relaxation increases. Now the relaxation curves are treated with a stretched exponential at the β parameter of 0.40−0.45, and T_1 times of 1.0 s for both lines (Figure 7). Generally speaking, such decrease in β could correspond to a more broad distribution of ^{1}H T_1 times,[50] which, in turn, shows that an amorphous character of the thermally treated sample is still present, even after 14 h. It should be noted that the relaxation curves obtained for the sample after its structural recovery are better treated with a biexponential function (Figure 7) to give a short and long ^{1}H T_1 components of 0.010−0.013 and 2.0 s for both resonances. Such short T_1 components could be attributed to very high proton mobility[52] or explained by the presence of

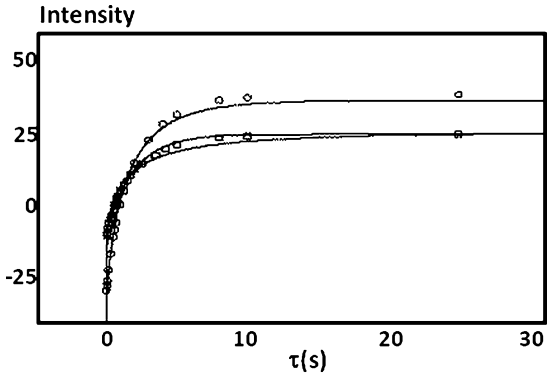

Figure 7. Relaxation curves in coordinates intensity (arbitrary units) vs delay time, τ (s), in the inversion−recovery experiments: the fresh-prepared ZnBP−NH_4 for signal at 7.1 ppm, where the solid line is the treatment with a stretched exponential (○); ZnBP−NH_4 after 14 h of heating, where the solid lines are the treatments with a stretched exponential and biexponential (□).

oxygen as paramagnetic centers. However, we believe that even in these terms, the smaller times are too short to be plausible.

In the frameworks of signal assignments, it is important to emphasize that according to careful inspection of the partially relaxed ^{1}H NMR spectra of ZnBP−NH_4 before and after heating, the line observed at 7.4 ppm is actually a superposition of three resonances at 8.0, 7.0, and 5.6 ppm (Figure 6). They can be assigned to protons of the C_6H_3 rings,[35] ions NH_4^+,[53,54] and H_2O molecules absorbed by the surface of ZnBP−NH_4. Thus, the thermal treatment of the sample does not eliminate NH_4^+ in accordance with an elemental analysis of ZnBP−NH_4 performed before and after heating. We believe that the NH_4^+ line is directly seen as a resonance at 6.6 ppm in the ^{1}H MAS NMR spectrum recorded just after heating (Figure 5). Then, the ^{1}H resonance observed for ZnBP−NH_4 before the thermal treatment at 3.6 ppm, which disappears just after heating and again appears in the spectrum after 14 h, necessary for structural recovery of ZnBP−NH_4, can be attributed to H_2O molecules in cavities located close to NH_4^+ ions (Figure 1). Due to this assignment and based on solid-state NMR data, we can conclude that the structural regularity of ZnBP−NH_4 is strongly supported by the P−O···$HN^+H^{\cdots}OH_2$ hydrogen-bonded network in cavities and elimination of the H_2O elements from this network is the driving force of the phase transition observed for ZnBP−NH_4, during its heating.

Finally, as we have shown above, all of the ^{1}H resonances in the fresh-prepared ZnBP−NH_4 relax very similarly with a relatively short T_1 time of 1.3−1.5 s. It is well-known that NH_4^+ ions and water molecules can undergo fast reorientations in such solids as ZnBP−NH_4 and even fast proton exchanges leading to proton conductivity.[51,55] These motions reasonably result in fast reorientations of their proton−proton dipolar vectors to cause the relatively fast ^{1}H spin−lattice dipole−dipole relaxation. It is obvious that these motions can remarkably reduce ^{1}H T_1 times for protons of rings C_6H_3 which are located in a structurally rigid parts of ZnBP−NH_4. Nevertheless, it seems to be unlikely that the C_6H_3 ^{1}H T_1 times can be equal to those for protons of NH_4^+ and H_2O. We assume that the effect is connected with spin diffusion, when spin flips for NH_4^+ are accompanied by spin flips of aromatic rings.[56]

In Situ X-ray Diffraction Studies. The in situ X-ray diffraction experiment of ZnBP−NH_4 was carried out to study

dx.doi.org/10.1021/cg400399v | Cryst. Growth Des. 2013, 13, 2973−2981

the reversible dehydration process. The X-ray diffractogram of the experiment shows a change in peak positions, with an increase in temperature to 200 °C and no change when cooled back to 25 °C (Figure 8). Upon exposure to water vapor, the

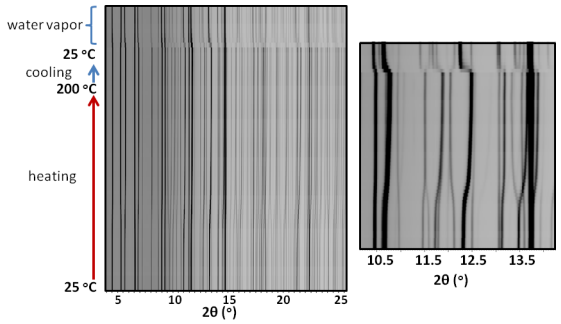

Figure 8. The diffractogram of the in situ hydration study (left) and a narrow 2θ region of the diffractogram giving a closer view of the change in the diffraction peaks for the reversible dehydration process (right).

peaks shift back quickly to their original positions, suggesting structural changes accompanied rehydration of the framework. Additionally, heating the sample to 80 °C also caused a shift in peak positions, which was reversible upon cooling back to 25 °C (Figure 9). Complementary to this, is the DSC curve, which

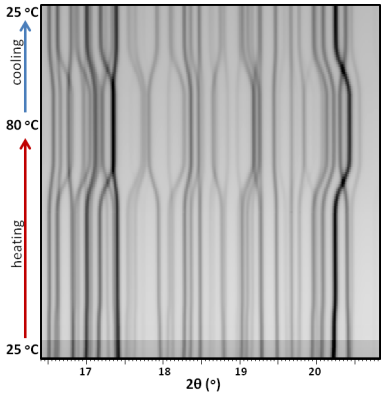

Figure 9. A diffractogram showing the reversible process upon heating to 80 °C and then cooling down to 25 °C.

indicates two endothermic phase transitions (Figure 10). From the in situ X-ray diffraction experiment, three phase changes occurred during the reversible dehydration process (Figure 11). The phase changes that occur: after heating to 45 °C, a phase change occurs without loss of solvent (phase II), continued heating to 120 °C resulted in a phase change with loss of solvent (phase III), and then rehydration occurs upon exposure to water vapor at 25 °C, resulting in the initial compound (phase I).

The structures for the different phases were determined from powder X-ray diffraction data, showing that the framework stays intact upon heating to 200 °C (Figures 12 and 13). The crystallographic parameters are similar for the three phases. Each phase crystallized in the orthorhombic *Ibam* space group and the asymmetric unit consists of two Zn(II) ions, one BTP molecule sited on a center of symmetry with one-half of the molecule as the asymmetric portion, and solvent molecules. For phase II at 60 °C, no loss of solvent occurs. The reversible

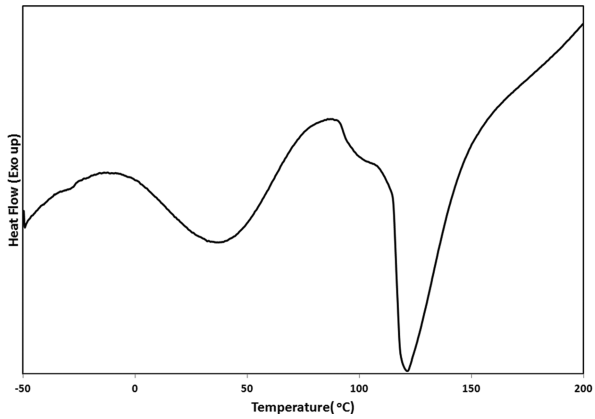

Figure 10. Differential scanning calorimetry analysis showing two endothermic phase changes.

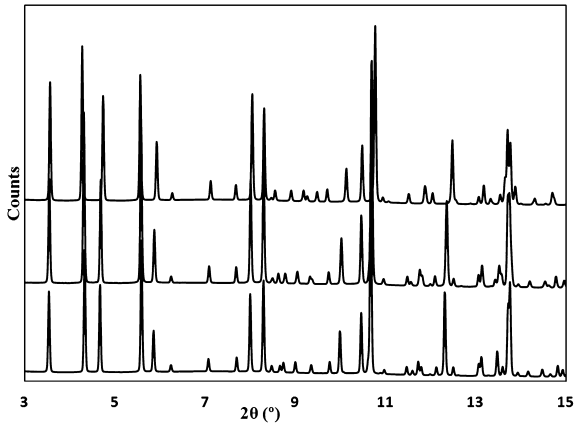

Figure 11. PXRD of the three different phases of ZnBP−NH_4: initial (bottom), 60 °C (middle), and 150 °C (top).

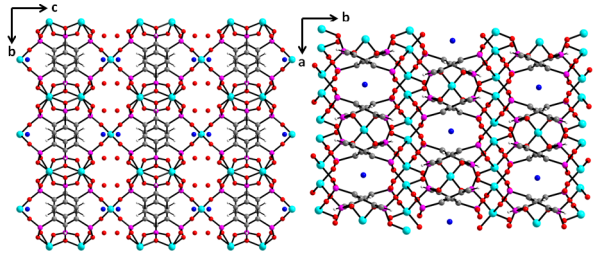

Figure 12. Views of the crystal structure along the *a* axis (left) and *c* axis (right) for compound ZnBP−NH_4-2, after heating to 60 °C (phase II). There, solvent molecules are disordered.

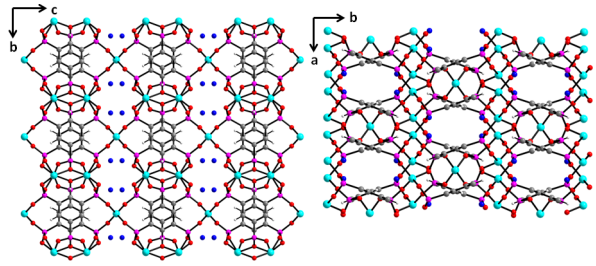

Figure 13. Views of the crystal structure along the *a* axis (left) and *c* axis (right) for compound ZnBP−NH_4-3, after heating to 150 °C (phase III).

dx.doi.org/10.1021/cg400399v | *Cryst. Growth Des.* 2013, 13, 2973−2981

solid−solid transition between phase I and phase II leads to enantiotropic polymorphs. The second solid−solid transition occurs at ∼120 °C, which is approximately where water loss occurs on the TGA. The structure of the phase III was determined at 150 °C. Water loss had occurred upon heating to this temperature; however, the ammonium ions were present in the larger pores.

The change in the free space of the crystal structure is reflected in the change of the unit cell parameters and volume. The plot of the normalized unit cell parameters and volume is given in Figure 14. A negative expansion is exhibited by the material as seen by a decrease in volume with an increase in temperature due to dehydration. All cell parameters decrease with an increase in temperature, except for the *b* axis. The *c* axis has the smallest change with a slight decrease which shortens the distance between the layers, narrowing the larger pores. Axis *b* lies parallel to the layers and is lengthened upon heating, elongating the larger pores. The *a* axis decreases the distance between the dimers, which decreases the distance between pillars (d···d distance = 8.443 and 8.296 Å, $\pi\cdots\pi$ = 3.720 and 3.669 Å, for phases II and III, respectively). This reduces the size of the smaller pore and no solvent molecules occupy this position.

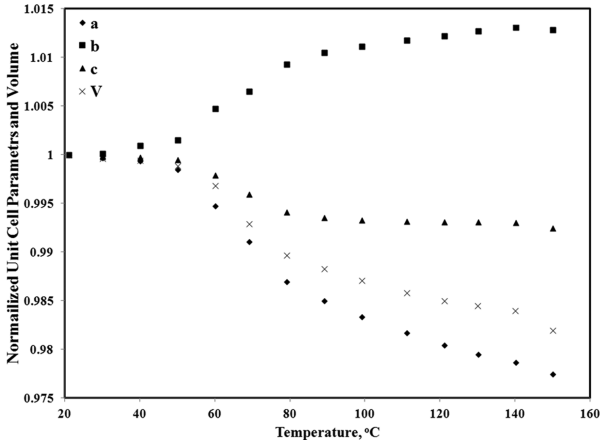

Figure 14. A plot showing the change in unit cell parameters and volume with increasing temperature. All data were normalized to the unit cell determined at room temperature.

DISCUSSION

The extension of the nonclassical organic−inorganic layered material,[32] PCMOF-3, to a 3D material was successful by a one-step hydrothermal synthesis. The layers are bridged by ZnO_4 centers to form an anionic framework. The bridged layers reduce the interlayer distance from 11.486 Å (PCMOF-3) to 9.908 Å. The decomposition of urea to ammonium provides the cations to help balance the −1 charge on the framework; however, some acidic protons are still present, giving the formula $Zn_{2.5}(H)_{0.4-0.5}(C_6H_3O_9P_3)(H_2O)_{1.9-2}(NH_4)_{0.5-0.6}$. This material has high thermal stability (∼600 °C based on TGA, Figure 4).

It is interesting that two synthetic approaches resulted in the same material. The topotactic pillaring approach of anionic layers provides the same anionic 3D framework in a two-step process.[37] It is thought that the zinc ions are partially dissolved from the anionic layers to form the anionic 3D framework.[37] This method provides a complete exchange of the acid protons in contrast to the one-step hydrothermal synthesis. However, the use of small amines in the hydrothermal synthesis in contrast to the large amines used in the topotactic pillaring approach, provides the 3D framework directly rather than the anionic layers.

The anionic framework has similarities to a copper-based MOF, synthesized using the BTP ligand.[35] An organic−inorganic layer is formed with Cu centers bridging the layers together. The layers consist of columns of dimers connected by Cu(II) ions. The dimers are not parallel to the layer due to the geometry of the metal centers. The Cu(II) ions have square pyramidal geometry and are coordinated to water molecules, which are directed into the pores. This leaves a small amount of free space in the pores in comparison to the ZnBP framework.

The ZnBP framework has two types of pores. The larger pores are interconnected by smaller pores in the [110] direction. The solvent molecules (water and ammonium ions) are disordered in ZnBP−NH_4; however, for ZnBP−CH_3NH_3 the $CH_3NH_3^+$ ion occupies the position in the smaller pore. On the basis of TGA, the NH_4^+ ions are not removed below 320 °C, indicating strong interactions with the framework. Both the solid state NMR and in situ X-ray diffraction experiments determined that NH_4^+ ions remained in the pores after dehydration.

A reversible dehydration process occurs with two phase transitions and reveals that the material exhibits negative expansion. The in situ X-ray diffraction study mapped both the changes in the framework and guest molecule positions, as the negative expansion process occurred (phase change). The first phase transition forms an enatiotropic polymorph. A slight decrease in volume is seen, but there is no large change in guest molecule positions. For the second phase transition, loss of water occurs and the NH_4^+ ions occupy the positions in the larger pore. These experiments suggest that the loss of hydrogen bonding due to water causes the contraction of the structure.

A less-coordinating cation would allow for easier removal, therefore the compound was synthesized with methyl ammonium ion (decomposition byproduct of 1,3-dimethylurea). The synthesis of an isostructural framework with different templating agents was successful. However, 25% less of the templating agent was present due to the larger size of the cation.

Replacement of the NH_4^+ ions through ion exchange is possible. Maeda and co-workers studied the cation exchange of ZnBP−NH_4 with alkali metal cations: Na^+, K^+, Rb^+, and Cs^+ ions.[36] A larger affinity for Rb^+ ions in aqueous alkali metal mixtures was determined due to cation size.[36] Maeda and co-workers did not investigate ion exchange with Li^+ ions. Our preliminary study resulted in ion exchange of the NH_4^+ with Li^+ ions. The ion-exchange reaction using $LiOH{\cdot}H_2O$, resulted in $Zn_{2.5}(C_6H_3O_9P_3)(H_2O)_2(Li)_{1.31}(OH)_{0.31}$, with all cation positions occupied with Li^+ ions.

Both PCMOF-3 and ZnBP have pores with water molecules, which could be used as proton conductors. A difference in proton conductivity should occur due to differences in mobility, type of charges, and structural differences in the framework. An increase in proton conductivity for the ZnBP−NH_4 phase is possible because of the decrease in size of the pores and thus an improved ion pathway.

Additionally, lithium ion conductivity could occur. In the dehydrated phase, free volume is lost and the Li^+ ions are believed to occupy the larger pores. This creates an improved

dx.doi.org/10.1021/cg400399v | *Cryst. Growth Des.* 2013, 13, 2973−2981

ion pathway and therefore the potential for lithium ion conductivity should increase. Conductivity studies still need to be investigated.

This material highlights that the negative expansion exhibited in MOFs, either by loss in some solvent molecules or by temperature, influences the positions of the guest molecules and thereby the possible applications due to the guest molecules.

CONCLUSION

The one-step hydrothermal synthesis resulted in isostructural materials with different cations: ZnBP−NH_4 and ZnBP−CH_3NH_3. The cations can be exchanged for lithium ions. The reversible dehydration process was studied by both in situ X-ray diffraction and solid-state NMR, which revealed two additional phases. The structures for all phases were determined (phases II and III). The reversible dehydration process caused the ZnBP framework to exhibit negative expansion due to a phase change. The loss in free volume forces the lithium or ammonium ions to occupy the larger pores in the dehydrated phase. Maximum lithium conductivity should be found in the dehydrated phase due to forced alignment of lithium ions in the pores. Studies pertaining to both proton and lithium conductivity for ZnBP are being pursued.

ASSOCIATED CONTENT

Supporting Information

Crystallographic tables (Tables S1 and S2), plots for Reitveld refinements are provided in Figures S1−S4, and PXRDs for ZnBP−NH_4 and ZnBP−Li (Figure S5). Structural information derived from the crystal structure refinements have been deposited at the Cambridge Crystallographic Data Center (e-mail: deposit@ccdc.cam.ac.uk) with CCDC file numbers 941753−941757. This material is available free of charge via the Internet at http://pubs.acs.org.

AUTHOR INFORMATION

Corresponding Author

*A.C.: e-mail, clearfield@chem.tamu.edu. T.L.K.: e-mail, tkinnibrugh@mail.chem.tamu.edu.

Notes

The authors declare no competing financial interest.

ACKNOWLEDGMENTS

This work was supported by the Robert A. Welch Foundation under Grant A0673 for which grateful acknowledgment is made. The authors are thankful for the support of Gregory Halder and 1-BM-C powder diffraction beamline, APS. Use of the Advanced Photon Source at Argonne National Laboratory was supported by the U.S. Department of Energy, Office of Science, Office of Basic Energy Sciences, under Contract DE-AC02-06CH11357. A.A.A. is grateful to the Fulbright Commission for the award of a Fellowship and to the University of Calabar for granting research leave.

ABBREVIATIONS

BTP, 1,3,5-benzenetriphosphonic acid; ZnBP, $Zn_{2.5}(C_6H_3O_9P_3)(H_2O)$; IRMOFS, isoreticular metal organic framework; ICP-AES, inductively coupled plasma-atomic emission spectroscopy; MAS, magic angle spinning

REFERENCES

(1) Li, J.-R.; Kuppler, R. J.; Zhou, H.-C. *Chem. Soc. Rev.* **2009**, *38*, 1477.
(2) Lee, J. Y.; Farha, O. K.; Roberts, J.; Scheidt, K. A.; Nguyen, S. B. T.; Hupp, J. T. *Chem. Soc. Rev.* **2009**, *38*, 1450.
(3) Wilmer, C. E.; Farha, O. K.; Yildirim, T.; Eryazici, I.; Krungleviciute, V.; Sarjeant, A. A.; Snurr, R. Q.; Hupp, J. T. *Energy Environ. Sci.* **2013**, *6*, 1158.
(4) Zhang, Z.; Zhao, Y.; Gong, Q.; Li, Z.; Li, J. *Chem. Commun. (Cambridge, U.K.)* **2013**, *49*, 653.
(5) Allendorf, M. D.; Bauer, C. A.; Bhakta, R. K.; Houk, R. J. T. *Chem. Soc. Rev.* **2009**, *38*, 1330.
(6) Kreno, L. E.; Leong, K.; Farha, O. K.; Allendorf, M.; Van, D. R. P.; Hupp, J. T. *Chem. Rev. (Washington, DC, U.S.)* **2012**, *112*, 1105.
(7) Long, J. R.; Yaghi, O. M. *Chem. Soc. Rev.* **2009**, *38*, 1213.
(8) Tan, J. C.; Cheetham, A. K. *Chem. Soc. Rev.* **2011**, *40*, 1059.
(9) Biswas, M. M.; Cagin, T. *Mater. Chem. Phys.* **2011**, *131*, 44.
(10) Reichenbach, C.; Kalies, G.; Lincke, J.; Laessig, D.; Krautscheid, H.; Moellmer, J.; Thommes, M. *Microporous Mesoporous Mater.* **2011**, *142*, 592.
(11) Chapman, K. W.; Sava, D. F.; Halder, G. J.; Chupas, P. J.; Nenoff, T. M. *J. Am. Chem. Soc.* **2011**, *133*, 18583.
(12) Chapman, K. W.; Halder, G. J.; Chupas, P. J. *J. Am. Chem. Soc.* **2008**, *130*, 10524.
(13) Chapman, K. W.; Halder, G. J.; Chupas, P. J. *J. Am. Chem. Soc.* **2009**, *131*, 17546.
(14) Barrera, G. D.; Bruno, J. A. O.; Barron, T. H. K.; Allan, N. L. *J. Phys.: Condens. Matter* **2005**, *17*, R217.
(15) Parise, J. B. *Rev. Mineral. Geochem.* **2006**, *63*, 205.
(16) Lind, C. *Materials* **2012**, *5*, 1125.
(17) Takenaka, K. *Sci. Technol. Adv. Mater.* **2012**, *13*, 013001/1.
(18) Lightfoot, P.; Woodcock, D. A.; Maple, M. J.; Villaescusa, L. A.; Wright, P. A. *J. Mater. Chem.* **2001**, *11*, 212.
(19) Miller, W.; Smith, C. W.; Mackenzie, D. S.; Evans, K. E. *J. Mater. Sci.* **2009**, *44*, 5441.
(20) Dubbeldam, D.; Walton, K. S.; Ellis, D. E.; Snurr, R. Q. *Angew. Chem., Int. Ed.* **2007**, *46*, 4496.
(21) Lock, N.; Christensen, M.; Wu, Y.; Peterson, V. K.; Thomsen, M. K.; Piltz, R. O.; Ramirez-Cuesta, A. J.; McIntyre, G. J.; Noren, K.; Kutteh, R.; Kepert, C. J.; Kearley, G. J.; Iversen, B. B. *Dalton Trans.* **2013**, *42*, 1996.
(22) Ogborn, J. M.; Collings, I. E.; Moggach, S. A.; Thompson, A. L.; Goodwin, A. L. *Chem. Sci.* **2012**, *3*, 3011.
(23) Lock, N.; Christensen, M.; Kepert, C. J.; Iversen, B. B. *Chem. Commun. (Cambridge, U. K.)* **2013**, *49*, 789.
(24) Zhao, L.; Yang, Q.; Ma, Q.; Zhong, C.; Mi, J.; Liu, D. *J. Mol. Model.* **2011**, *17*, 227.
(25) Lock, N.; Wu, Y.; Christensen, M.; Cameron, L. J.; Peterson, V. K.; Bridgeman, A. J.; Kepert, C. J.; Iversen, B. B. *J. Phys. Chem. C* **2010**, *114*, 16181.
(26) Mu, B.; Walton, K. S. *J. Phys. Chem. C* **2011**, *115*, 22748.
(27) Zhou, W.; Wu, H.; Yildirim, T.; Simpson, J. R.; Hight, W. A. R. *Phys. Rev. B: Condens. Matter Mater. Phys.* **2008**, *78*, 054114/1.
(28) Ponomareva, V. G.; Kovalenko, K. A.; Chupakhin, A. P.; Dybtsev, D. N.; Shutova, E. S.; Fedin, V. P. *J. Am. Chem. Soc.* **2012**, *134*, 15640.
(29) Hurd, J. A.; Vaidhyanathan, R.; Thangadurai, V.; Ratcliffe, C. I.; Moudrakovski, I. L.; Shimizu, G. K. H. *Nat. Chem.* **2009**, *1*, 705.
(30) Sen, S.; Nair, N. N.; Yamada, T.; Kitagawa, H.; Bharadwaj, P. K. *J. Am. Chem. Soc.* **2012**, *134*, 19432.
(31) Wei, M.; Wang, X.; Duan, X. *Chem.—Eur. J.* **2013**, *19*, 1607.
(32) Taylor, J. M.; Mah, R. K.; Moudrakovski, I. L.; Ratcliffe, C. I.; Vaidhyanathan, R.; Shimizu, G. K. H. *J. Am. Chem. Soc.* **2010**, *132*, 14055.
(33) Maeda, K.; Hatasawa, H.; Kawawa, K.; Nagayoshi, N.; Matsushima, Y. *Chem. Lett.* **2011**, *40*, 215.
(34) Araki, T.; Kondo, A.; Maeda, K. *Chem. Commun. (Cambridge, U.K.)* **2013**, *49*, 552.

(35) Kong, D.; Zoñ, J.; McBee, J.; Clearfield, A. *Inorg. Chem.* **2006**, *45*, 977.
(36) Maeda, K.; Takamatsu, R.; Mochizuki, M.; Kawawa, K.; Kondo, A. *Dalton Trans.* 2013, submitted.
(37) Maeda, K.; Kondo, A. *Dalton Trans.* 2013, submitted.
(38) SAINTP+, B. Bruker AXS: Madison, Wisconsin, 2005.
(39) SADABS-2008/1, B. Bruker AXS: Madison, Wisconsin, 2008.
(40) Sheldrick, G. M. In *Structure Determination Software Suite*, 2008/4 ed.; SHELXTL: Madison, Wisconsin, 2008.
(41) Brandenburg, K.; Berndt, M. *DIAMOND*; Crystal Impact GbR: Bonn, Germany, 1999.
(42) Macrae, C. F.; Edgington, P. R.; McCabe, P.; Pidcock, E.; Shields, G. P.; Taylor, R.; Towler, M.; van de Streek, J. *J. Appl. Crystallogr.* **2006**, *39*, 453.
(43) Chupas, P. J.; Chapman, K. W.; Kurtz, C.; Hanson, J. C.; Lee, P. L.; Grey, C. P. *J. Appl. Crystallogr.* **2008**, *41*, 822.
(44) Coelho, A. A.; Kern, A. *CPD Newsletter* **2005**, *32*, 43.
(45) Bruker, 4.2 ed.; Bruker AXS: Karlsuhe, Germany, 2009.
(46) Le Bail, A.; Duroy, H.; Fourquet, J. L. *Mater. Res. Bull.* **1988**, *23*, 447.
(47) Favre-Nicolin, V.; Cerny, R. *J. Appl. Crystallogr.* **2002**, *35*, 734.
(48) Fox, Free Objects for Crystallography, http://objcryst.sourceforge.net.
(49) Petricek, V.; Dusek, M.; Palatinus, L. *The Crystallographic Computing System*; Institute of Physics: Praha, Czech Republic, 2006.
(50) Bakhmutov, V. I. *Solid-State NMR in Materials Science: Principles and Applications*; CRC: Boca Raton, FL, 2011.
(51) Slade, R. C. T.; Forano, C. R. M.; Peraio, A.; Alberti, G. *Solid State Ionics* **1993**, *61*, 23.
(52) Zima, V.; Svoboda, J.; Melanova, K.; Benes, L.; Casciola, M.; Sganappa, M.; Brus, J.; Trchova, M. *Solid State Ionics* **2010**, *181*, 705.
(53) Haase, F.; Sauer, J. *J. Phys. Chem.* **1994**, *98*, 3083.
(54) Ma, D.; Han, X.; Xie, S.; Bao, X.; Hu, H.; Au-Yeung, S. C. F. *Chem.—Eur. J.* **2002**, *8*, 162.
(55) Afanassyev, I. S.; Moroz, N. K. *Solid State Ionics* **2003**, *160*, 125.
(56) Morris, W.; Taylor, R. E.; Dybowski, C.; Yaghi, O. M.; Garcia-Garibay, M. A. *J. Mol. Struct.* **2011**, *1004*, 94.